Ecological Engineering & Environmental Technology, 2025, 26(12), 376–392 https://doi.org/10.12912/27197050/214068 ISSN 2719–7050, License CC-BY 4.0

Received: 2025.10.23 Accepted: 2025.11.15 Published: 2025.12.01

Utilization of satellite imagery for drought identification and drought susceptibility maps via the frequency ratio

Thamrin Putri Saridayana¹, Mukrimin², Soma Andang Suryana²

- ¹ Forestry Master Program, Faculty of Forestry, Hasanuddin University, 90245, Makassar, Indonesia
- ² Department of Forestry, Faculty of Forestry, Hasanuddin University, 90245, Makassar, Indonesia
- * Corresponding author's e-mail: mukrimin@unhas.ac.id

ABSTRACT

Despite substantial land cover changes and a history of recurrent droughts, the Bila watershed has not been subjected to comprehensive spatial drought vulnerability. This study overcomes this research gap by integrating a geographic information system (GIS) with the frequency ratio (FR) method to produce an accurate and scientifically based map of drought-prone zones. To the best of the authors' knowledge, this study is the first to apply the FR method to assess drought vulnerability at the watershed scale in South Sulawesi, thus contributing a new and data-driven framework to advance spatial drought analysis in the tropical environments. The FR analysis used seven drought-related factors: rainfall, land cover, building density, hotspots, vegetation density, slope, and river distance. The results of the LST analysis revealed that approximately 43.25% of the area in the Bila watershed experienced drought, primarily due to moderate building density and residential land cover, as indicated by high FR values of 2.98 and 2.89, respectively. The results of mapping the Bila watershed's drought-prone zones show that areas with high to very high drought vulnerability categories tend to be concentrated in paddy fields, residential areas, dryland agriculture, and areas with moderate building density. The spatial distribution pattern reveals that the downstream areas of the Bila watershed exhibit a greater level of drought vulnerability than the upstream regions do.

Keywords: drought vulnerability, Bila watershed, remote sensing, geographic information systems, land surface temperature, frequency ratio.

INTRODUCTION

The Intergovernmental Panel on Climate Change (IPCC) in 2023 predicts that the global temperature increase will reach or exceed 1.5 °C or 2.7 °F between 2021 and 2040. According to Thomas et al. (2014), tropical countries, including Indonesia, are vulnerable to hydrometeorological disasters, such as droughts triggered by climate change. The phenomenon of drought in tropical regions not only threatens food security, but also has direct implications for the availability of water, land degradation, and socio-economic stability of the community.

Research on drought has been conducted in several tropical countries, including the Philippines, especially in the Ilocos Norte region (Alonzo et al., 2023), India (Chuphal et al., 2024),

Malaysia (Hasan et al., 2021), Brazil (Cunha et al., 2019), and Indonesia (Amalo et al., 2018; Nursaputra et al., 2021). However, most of these studies focused on a national or regional scale without detailed spatial mapping at the watershed level. In fact, watersheds are an ideal hydrological unit for understanding the interaction between biophysical factors and human activity on drought dynamics.

The Bila watershed is one of the watersheds in South Sulawesi that administratively crosses Sidrap, Wajo, and Enrekang Regencies. Research by Rahmat et al. (2023) indicated that the Bila watershed has experienced significant changes in land cover, with approximately 915.96 hectares of secondary forest converted to agricultural land. A 0.7% decrease in forest cover could substantially reduce water availability and increase surface runoff by up to 45% (Garg et al., 2019). The

increased runoff contributes to sedimentation in Lake Tempe, which serves as the main reservoir for flows from the Bila watershed, thereby reducing water tamping capacity and increasing the risk of drought and flooding. According to Cahyono et al. (2024), the annual sediment thickness in Lake Tempe ranges from 20–40 cm.

Historical data on drought events in South Sulawesi from the National Disaster Management Agency (BNPB) show that from 2000–2023, 169 drought events occurred. The Central Statistics Agency noted that the 2023 drought affected and displaced 211,086 people, with 11,582 of them residing in the Wajo and Sidrap Regencies. However, there has not been a comprehensive spatial study of drought-prone zones in the Bila watershed. This information is important to support mitigation and early warning strategies, considering that this region plays a strategic role in providing water for Lake Tempe and the surrounding area.

Previous research in South Sulawesi, Indonesia generally used drought indices (Nursaputra et al., 2021; Senjani et al., 2020), but has not integrated spatial statistical approaches to quantitatively assess vulnerability. In addition, most studies focus only on drought intensity, without considering biophysical and land use factors that contribute to the region's vulnerability to drought. This gap demonstrates the need for more objective and probabilistic-based mapping methods to assess drought vulnerability spatially.

The frequency ratio (FR) method is known to have a high level of precision in disaster vulnerability assessment based on spatial data (Lee et al., 2012). The FR method has been widely used in landslide vulnerability mapping (Addis, 2023; Cantarino et al., 2023), flood hazard analysis (Rahmati et al., 2015; Wang et al., 2021), and soil erosion studies (Islam et al., 2022), but its application in drought vulnerability mapping is still very limited. Therefore, this study seeks to bridge this gap by applying the FR method to identify the factors that have the most influence on drought vulnerability in the Bila watershed. Specifically, this study aims to identify the main factors contributing to drought in the Bila Watershed and applying the FR method in spatial mapping of drought susceptibility.

The novelty of this study lies in the application of the FR method in mapping drought vulnerability at the watershed level, which has not been widely done in the tropical context of Indonesia. The results of this research are expected to strengthen the scientific basis in the development of early warning systems and climate change adaptation strategies in the Bila watershed area and its surroundings.

MATERIALS AND METHODS

Study area

The object of this research is the Bila watershed, which is located in South Sulawesi, Indonesia, within the administrative boundaries of the Sidenreng Rappang, Wajo, and Enrekang Regencies. The area covers approximately 158,784 ha, on the basis of the results of the delineation of the watershed from the digital elevation model (DEM) by the author via GIS software (2024). Geographically, the research area is located 3°34'16.69"–3°48'28.26" S and 120°03'23.33"–120°02'04.58" E (Google Earth, 2024). The topography of the area varies, ranging from lowlands to hills. Most of the area is dominated by the slope class 0–8% (flat category). The average annual rainfall in the region ranges from 1.800–3.000 mm a year.

Identification of drought using land surface temperature

The drought identification process was carried out by downloading Landsat 8 OLI/TIRS imagery during the dry season from the 2019–2023, then performing radiometric and atmospheric corrections. Land surface temperature (LST) was calculated using Band 10 (Thermal Infrared Sensor/TIRS) followed the Avdan and Jovanovska (2016) algorithm, resulting in an LST raster in degree Celcius. The LST values were then classified according to Liviona et al. (2020), namely <20 °C (very low), 20–25 °C (low), 25–30 °C (medium), and 30–35 °C (high). Next, the LST classes were reclassified into two main gorup, namely the nondrought category (classes <20 °C and 20–25 °C) and the drought category (classes 25-30 °C and 30-35 °C). The classification raster was then converted to shapefile format, and only areas included in the drought category were extracted for each year of observation. All annual drought shapefiles from 2019-2023 were then overlaid gradually to produce a single layer depicting the spatial distribution on drought events in the Bila Watershed during the study period.

Collecting data on drought factors

Rainfall

Rainfall data was obtained from NASA/POWER CERES/MERRA-2 satellites through the data access viewer page (accesed January 18, 2025). Eight coordinates were selected to represent the spatial distribution of the Bila Watershed, and each was used as a point for downloading daily rainfall data. The daily data were then checked to ensure there were no missing values or anomalies, and then summed to obtain the

annual rainfall at each station point. The annual rainfall values were integrated into GIS software and mapped using the Thiessen Polygon method to produce a spatial distribution of rainfall representing the area of influence of each station. The resulting polygons were converted into rasters and classified according to Riajaya et al. (2024) into four classes: 1.500–2.000 mm, 2.000–2.500 mm, 2.500–3.000 mm, and >3.000 mm (Figure 1). This classified rainfall raster was used as one of the factors in calculating the drought susceptibility index.

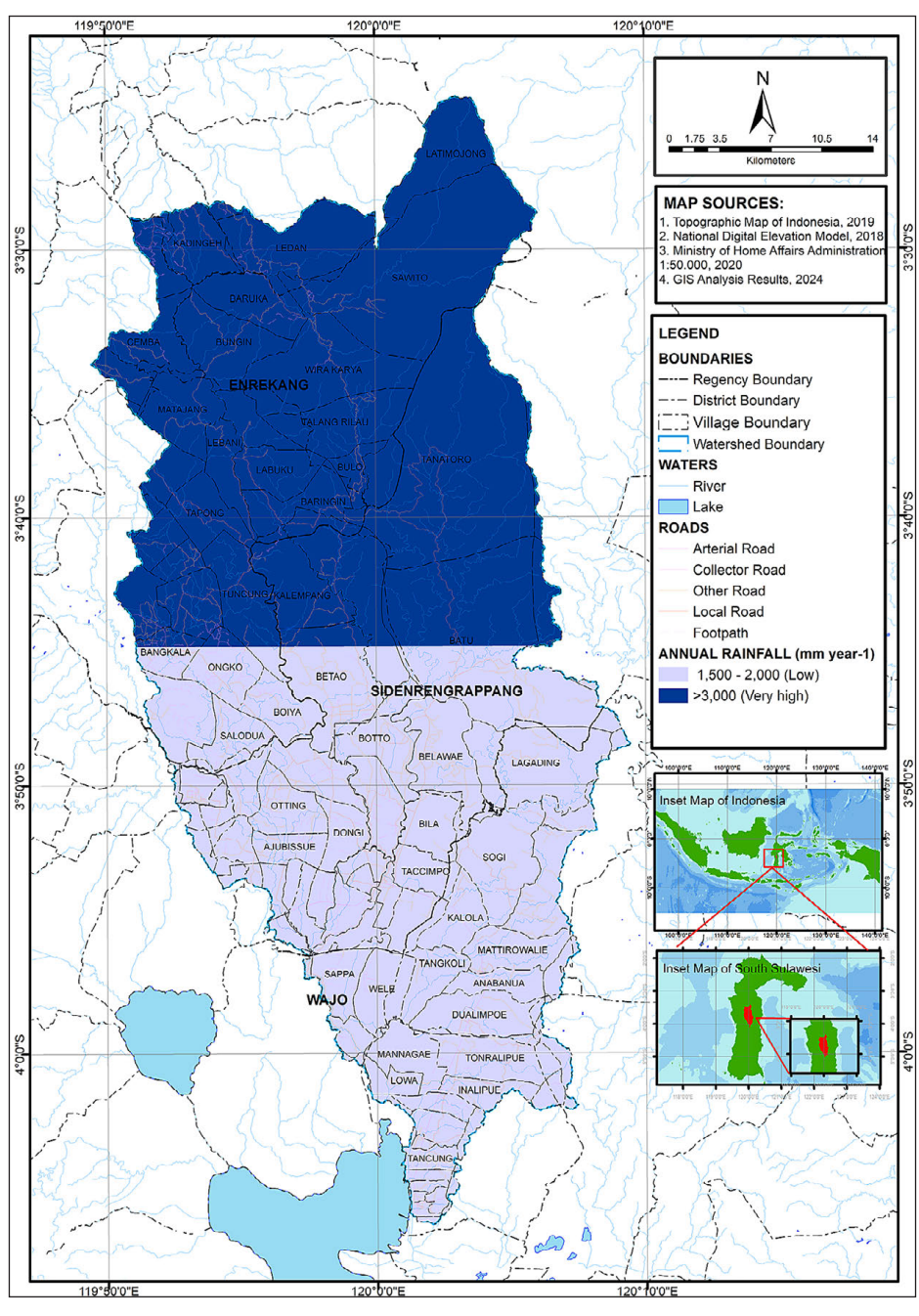


Figure 1. Rainfall factor (source: NASA Power (CERES/MERRA-2))

Land cover

Land cover data were generated through a visual interpretation of Landsat 8 OLI/TIRS imagery. Prior to interpretation, the imagery was preprocessed through radiometric and atmospheric correction, subsetting to the Bila Watershed boundaries, and reprojection to UTM WGS 84 Zone 51S. The interpretation process was conducted using on-screen digitizing in GIS software, in which land cover classes were delineated based on spectral characteristics, tone, texture, pattern, and contextual information. High-resolution

basemaps from Google Earth were used to support the identification of land cover boundaries and improve the reliability of class labeling. Each digitized polygons was assigned a land cover category and subsequently underwent topology checks to ensure spatial consistency, eliminate gaps and overlaps, and correct sliver polygons. The resulting land cover map was produced at cartographic scale of 1:50,000 and subsequently converted into raster format (30 m resolution) for use as an input factor in the drought susceptibility index (Figure 2).

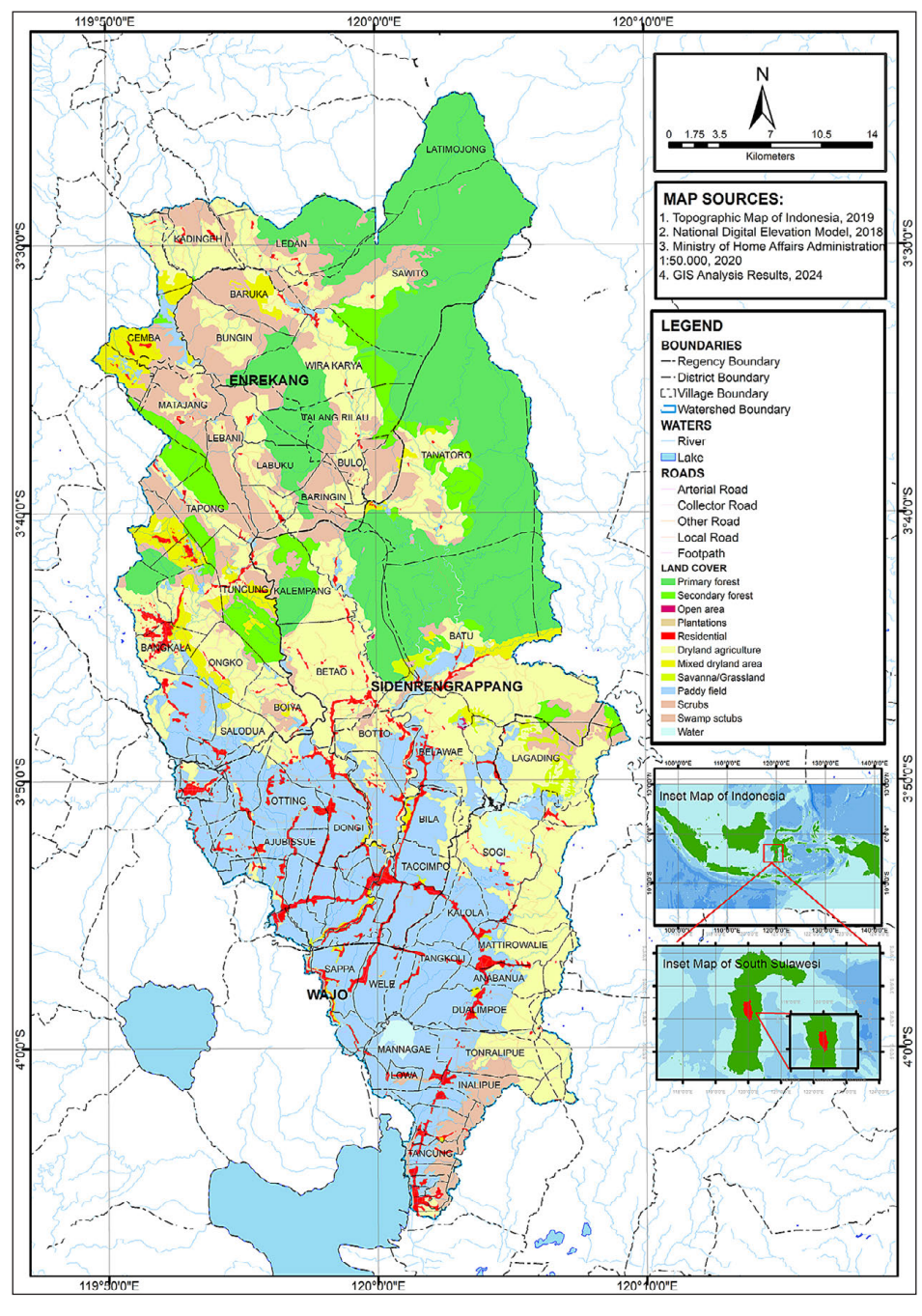


Figure 2. Land cover factor (source: Landsat 8 OLI/TIRS)

Building density

Building density in the Bila Watershed was derived from Landsat 8 OLI imagery using the Normalized Difference Built-up Index (NDBI). The analysis began by downloading cloud-free Landsat 8 imagery that had undergone radiometric and atmospheric correction. The surface reflectance values of Band 6 *SWIR1) and Band 5 (NIR) were then extracted, as these bands are required for NDBI computation. After preprocessing, the NDBI values were calculated in GIS software using the formula propsed by Zha et al. (2003), where:

$$NDBI = \frac{(\rho SWIR1 - \rho NIR)}{(\rho SWIR1 + \rho NIR)} \tag{1}$$

where: on Landsat 8: $\rho SWIR1$ – Band 6 (shortwave infrared); ρNIR – Band 5 (near infrared).

The resulting NDBI raster was inspected to ensure that no errors were present, and was then classified into four density categories following commonly applied thresholds: -1 to 0 for non-building areas, 0 to 0.1 for low building density, 0.1 to 0.2 for moderate building density, and 0.2 to 1 for high building density (Figure 3).

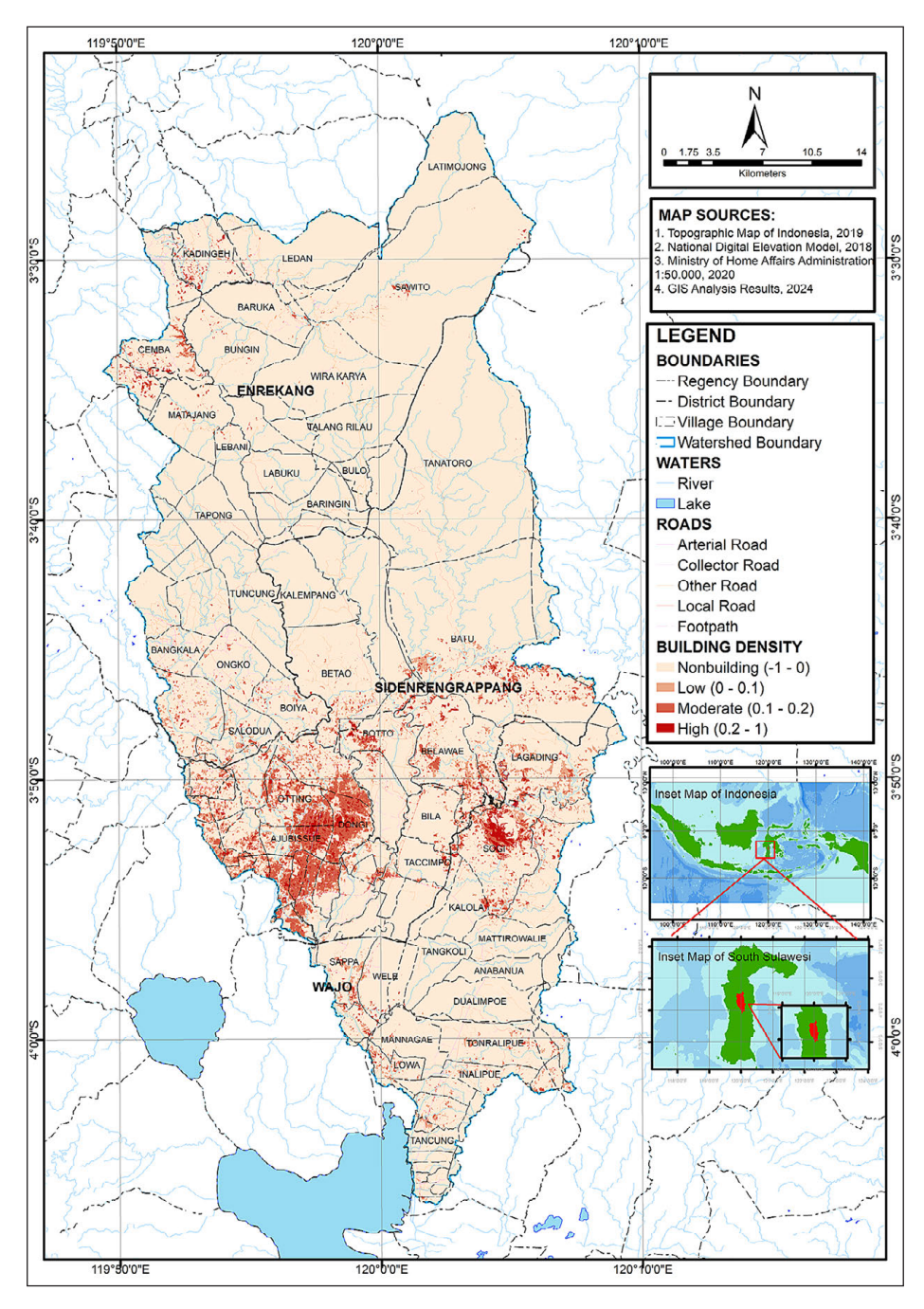


Figure 3. Building density factor (source: Landsat 8 OLI)

Hotspot

Hotspot data were obtained from NOAA-20 VIIRS imagery (375 m resolution) through the FIRMS platform (the https://firms.modaps.eos-dis.nasa.gov, accessed December 11, 2024). All hotspot points within the Bila Watershed were extracted and imported into GIS software for further analysis. To examine the spatial concentration of fire occurrences, a Getis-Ord Gi* hotspot analysis was performed, producing Z-score values that represent statistically significant clusters of high or low. The resulting Z-score layer was then interpolated using the inverse distance weighting (IDW) method to generate a continuous

raster surface depicting the intensity of fire activity across the watershed. The interpolated Z-score raster was subsequently classified into five hotspot values categories: <-1 (very low), -1 to 0 (low), 0–1 (moderate), 1–2 (high), and >2 (very high) (Figure 4).

Density of vegetation

Vegetation density was assessed using the normalized difference vegetation index (NDVI) derived from Landsat 8 OLI imagery. After preprocessing the imagery, surface reflectance values for Band 5 (NIR) and Band 4 (Red) were extracted.

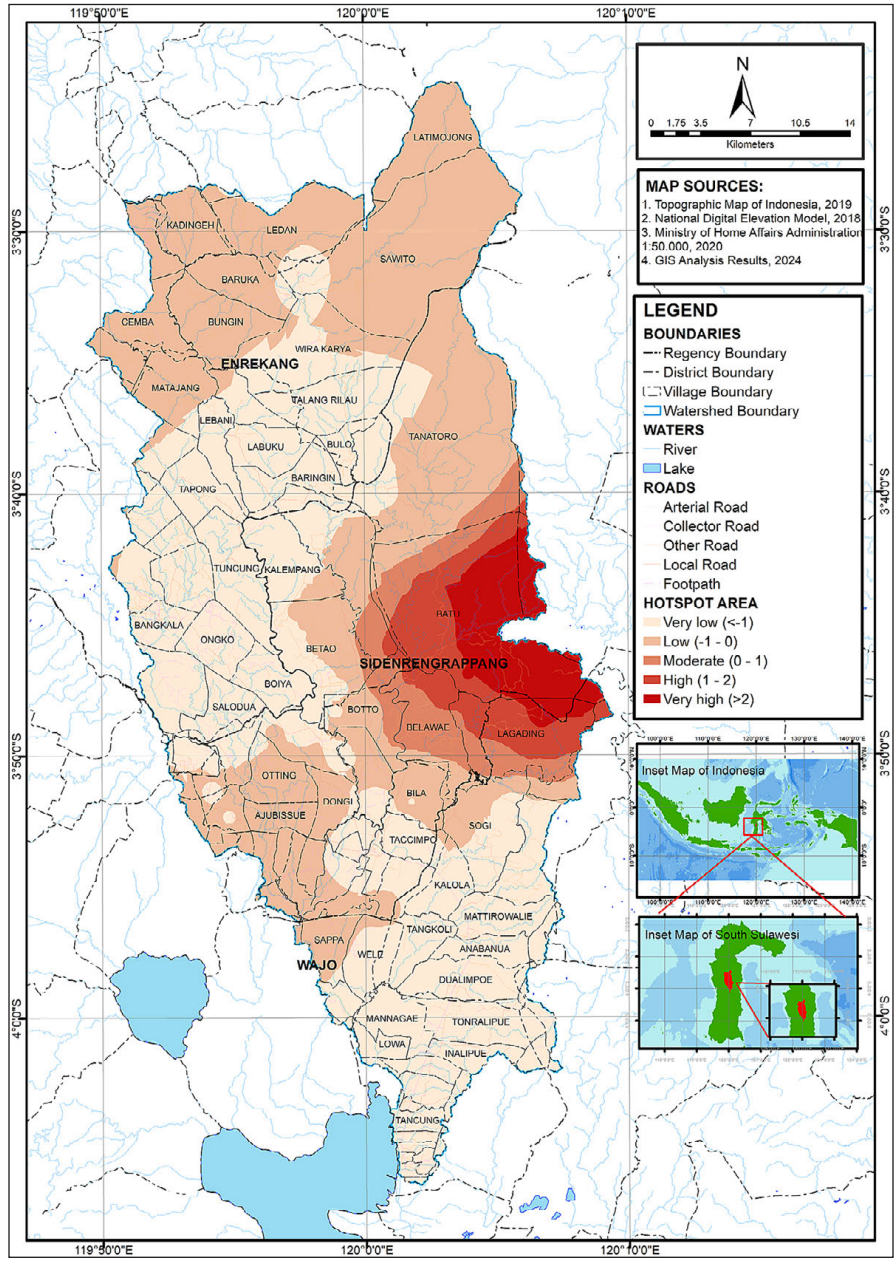


Figure 4. Hotspot factor (source: NOAA-20 VIIRS)

NDVI was calculated in GIS software following the standard formula (Shashikant et al., 2021):

$$NDVI = \frac{(\rho NIR - \rho Red)}{(\rho NIR + \rho Red)}$$
 (2)

where: ρNIR – Band 5 (near infrared) and ρRED – Band 4 (red).

The resulting NDVI raster was examined to ensure data quality and then classified according to the thresholds recommended by Ahmed and Singh (2020), where NDVI values <0.125 represent non-vegetated areas (water/open land), values between 0.125 and 0.25 indicate sparse vegetation, values between 0.25 and 0.5 indicate

moderate vegetation, and values >0.5 represent dense vegetation (Figure 5). This classified NDVI raster provided a spatial representation of vegetation cover conditions in the watershed and was included as an input factor in the drought susceptibility modeling.

Slope

Slope was obtained from the digital elevation model (DEM) and processed in GIS software. The DEM was first preprocessed to ensure that its spatial extent and projection matched the boundary of the Bila Watershed. Using the slope analysis tool, the terrain slope for each

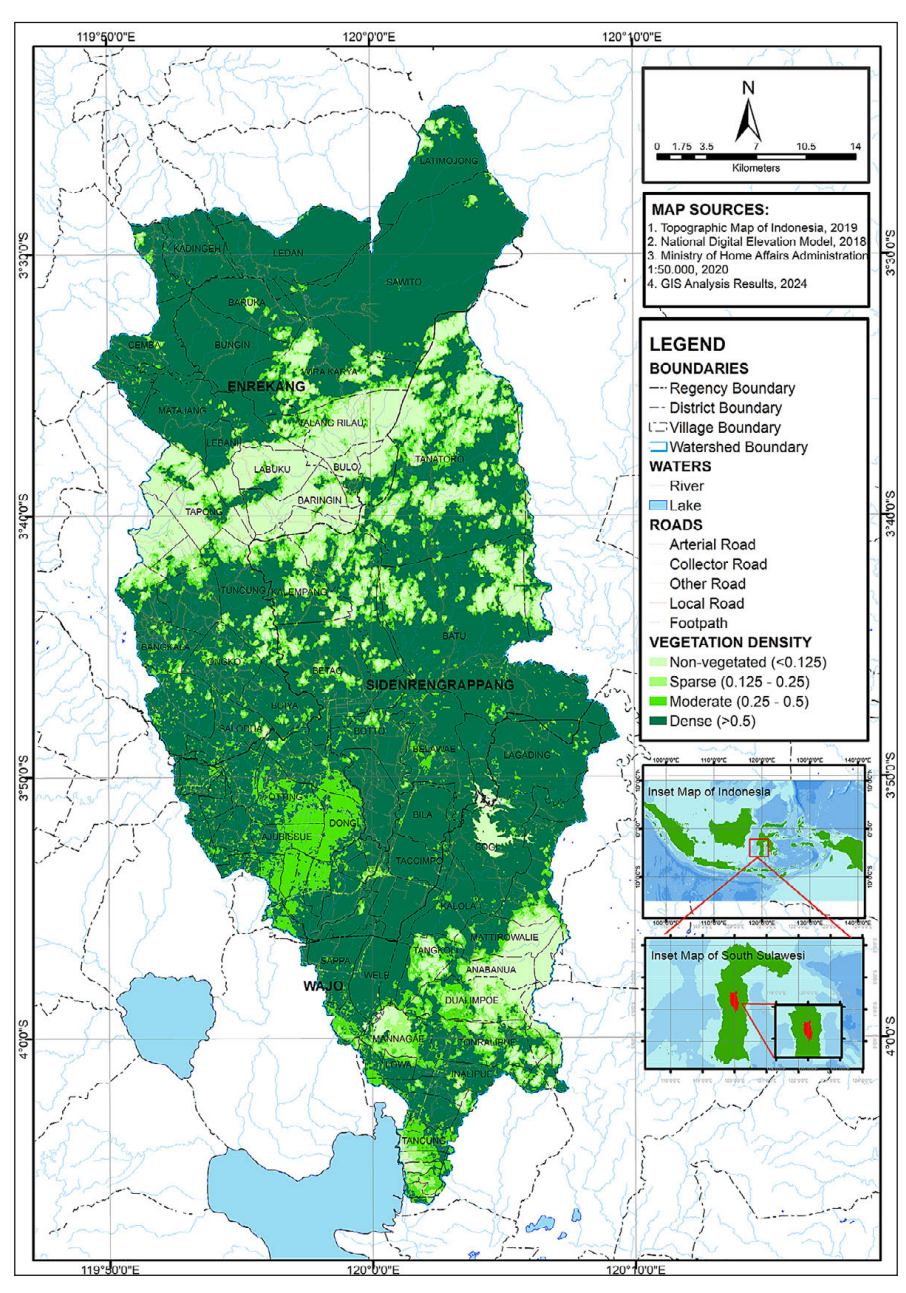


Figure 5. Vegetation density factor (source: Landsat 8 OLI)

pixel was computed and expressed as a percentage. The resulting slope raster was then classified following the criteria of Utama and Indriani (2021), which categorize slope into five classes: 0–8% flat, 8–15% sloping, 15–25% moderately steep, 25–45% steep, and >45% very steep (Figure 6). This classified slope map provided a spatial representation of terrain variability across the watershed and was incorporated as one of

the physical conditioning factors in the drought susceptibility analysis.

River distance

The river distance factor was generated using river network data obtained from the Indonesian Topographic Map produced by the Geospatial Information of Agency. The river shapefile was first clipped to match the boundary of the Bila

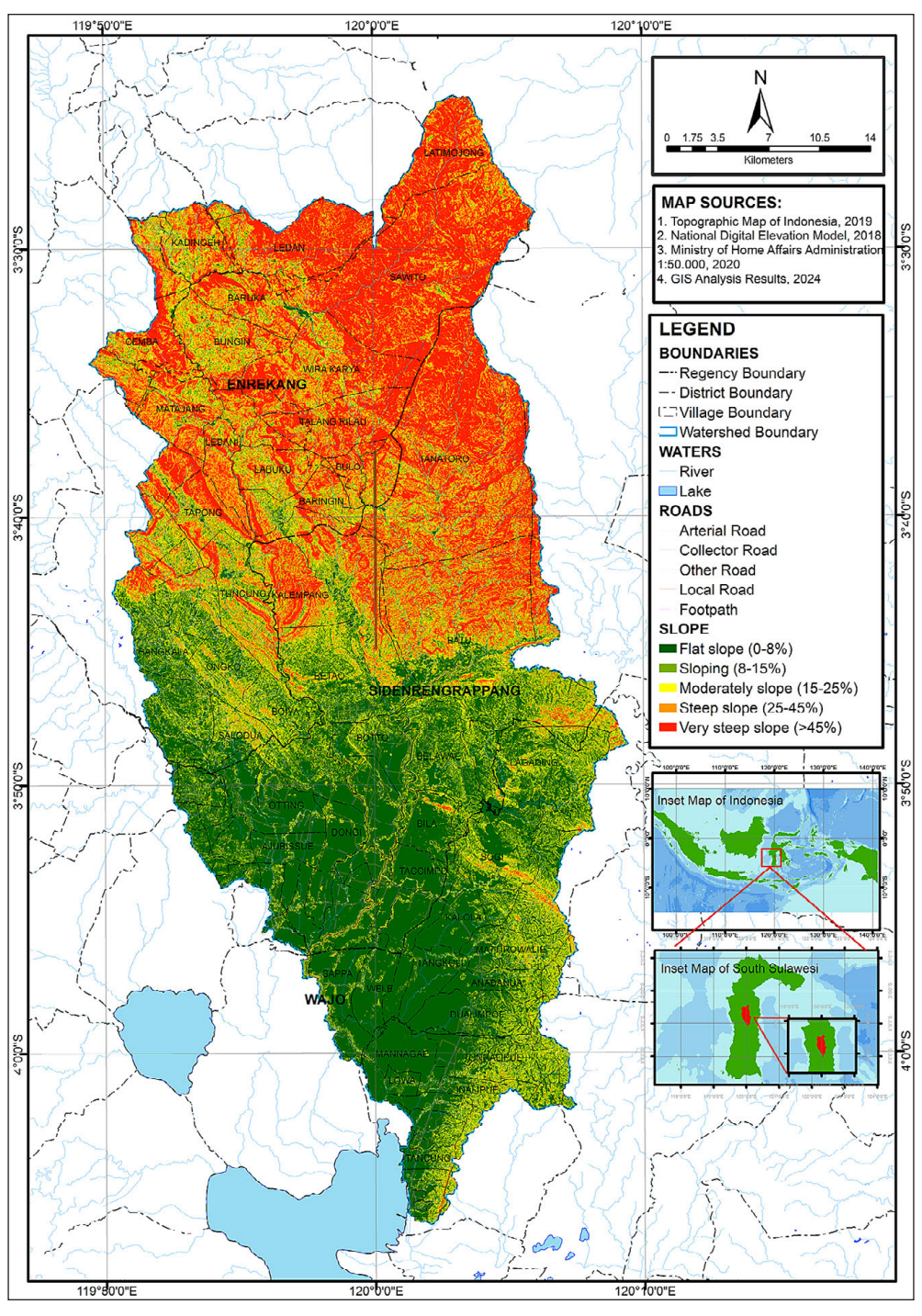


Figure 6. Slope factor (source: digital elevation model (DEM))

Watershed to ensure spatial consistency. Using the Euclidean Distance tool in GIS software, a continuous raster surface was produced to represent the straight-line distance from each pixel to the nearest river channel. The resulting distance raster was then classified into four categories based on the criteria of Prasetyo et al. (2018), namely 0–100 m, 100–250 m, 250–500 m, and >500 m (Figure 7). These categories capture the spatial gradient of proximity to river systems, which may influence

local water availability and contribute to drought susceptibility patterns across the watershed.

Drought mapping via the frequency ratio

The frequency ratio (FR) method was applied to quantify the relationship between historical drought occurrences and the conditioning factors used in this study. This method is widely recognized for its precision in vulnerability assessment

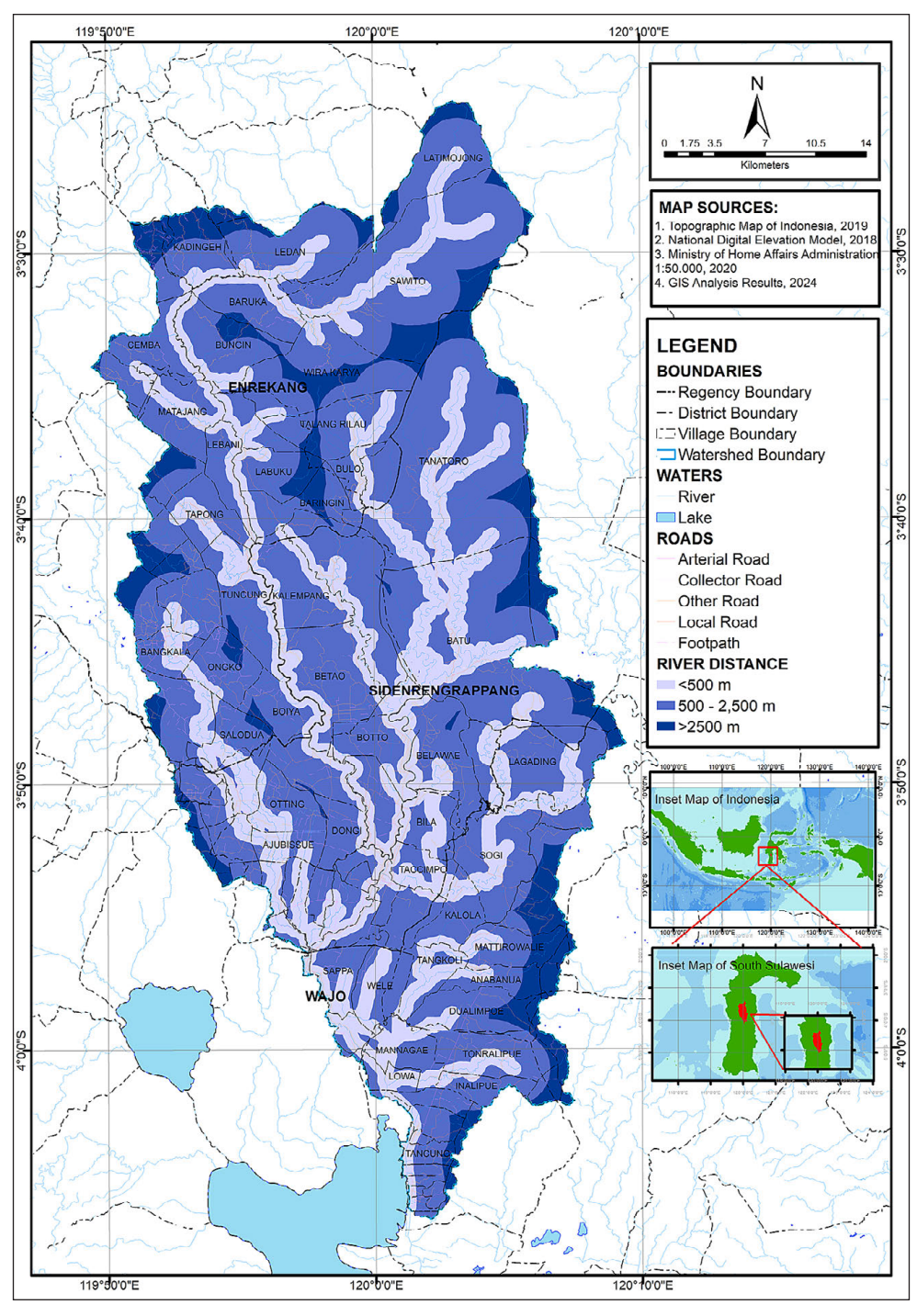


Figure 7. River distance factor (source: Geospatial Information Agency)

because it measures the likelihood of drought occurrence within each class of a causative factor compared to its overall spatial distribution (Lee et al., 2012). In this study, the FR modeling procedure was carried out through the following steps:

- Preparation of drought occurrence data the final drought map derived from LST analysis (2019–2023) was first converted from raster format to point data using the Raster to Point tool. Each point represents a location where drought was recorded. These points served as the event layer required for FR calculation.
- 2. Extraction of causative factor values each conditioning factor was converted to a classified raster. The values of all factors were then extracted to each drought occurrence point using the Extract Multivalue to Points function in GIS. This process generated a table indicating how many drought events occurred in each factor class.
- 3. Calculation of pixel distribution for each factor class − for each conditioning factor, the total number of pixels in each class (PnxL) and the total number of pixels in the entire watershed (∑Pnx) were computed. This step quantifies the spatial proportion of ach factor class.
- 4. FR calculation the Fr value for each class was calculated using the formula (Soma and Kubota, 2017):

$$FR = \frac{PxcL (nm)/\sum PnxL}{Pixel (nm)/\sum Pnx}$$
 (3)

where: PxcL – number of instances in the n class of parameter m (nm); Pixels – the number of pixels in the n class with the parameter m (nm); $\Sigma PnxL$ – total pixel parameter m; ΣPnx – total pixel area.

Classes with FR>1 indicate a positive or strong correlation with drought occurrence, while FR<1 indicates a weak association.

Construction of FR raster layers

Each factor's FR values were assigned back to their corresponding classes to produce FR-based raster maps for all conditioning factors.

Development of the drought susceptibility index (DSI)

All FR rasters were combined using Raster Calculator tool in GIS software to produce the DSI:

$$DSI = FR1 + FR2 + \dots + FRn \tag{4}$$

where: *FR*1, *FR*2, and *FRn* are the frequency ratios for the factor.

This additive approach reflects the cumulative influence of all drought-related factors.

Classification of DSI into susceptibility levels

The final DSI raster was classified into five drought susceptibility categories: very low, low, moderate, high, and very high using the Natural Break (Jenks) algorithm in GIS software.

Data validation

The statistical evaluation aimed to evaluate the predictive performance and reliability of the drought vulnerability models developed in this study. The main hypothesis is that the FR-based model is able to significantly differentiate between drought-prone and non-drought-prone areas.

Data on drought events for the 2019–2023 period are compiled and combined into one layer of drought events. The data are then classified into two categories, drought (value = 1) and non-drought (value = 0), and converted into a point shapefile (.shp). This dataset was randomly divided into two subsets: 70% (388,208 points) were used for model training, and the remaining 30% (157,803 points) were used for validation to evaluate the predictive performance of drought vulnerability models.

The next step involves extracting raster values through the Extract Value to Points function in GIS software. In this process, the drought event point shapefile is used as the servest as the point feature, while the vulnerability map in raster (.tif) format is used as the input raster. This operation generates a dataset containing raster values that correspond to each drought occurrence point.

The extracted data is then imported into the SPSS software (version 20) for analysis. Receiver operating characteristic (ROC) analysis is performed to evaluate the model's performance. In this analysis, the raster value serves as the test variable, while the drought classification serves as the status variable. The area under the curve value (AUC) obtained from this analysis is used to assess the model's accuracy in predicting drought-prone areas. Based on the classification standards from previous research (Balamurugan et al., 2017), the AUC values are interpreted as follows: excellent (0.9–1.0), excellent (0.8–0.9),

good (0.7–0.8), average (0.6–0.7), and poor (0.5–0.6). To assess the statistical significance of AUC results, a z-test is applied to test the null hypothesis (H0: AUC = 0.5). P-value < 0.05 indicates that the model performs significantly better than the random classification. In addition, the accuracy of the model is compared between training and validation datasets to test possible overfitting.

RESULTS AND DISCUSSION

Drought from the LST

The LST in 2019 reached 35 °C, followed by 29 °C in 2020, 28 °C in 2021, and 32 °C in 2022 and 2023 (Figure 8) on the basis of the analysis of Landsat 8 OLI/TIRS images. According to records for the 2015–2019 period, 2019 was one of the hottest years. This finding is supported by Yuniasih et al. (2023), who reported that Indonesia experienced an El Niño event in 2019, although it was weaker than it was from 2015–2016. These findings support the results of this study, suggesting that the highest temperatures during the study

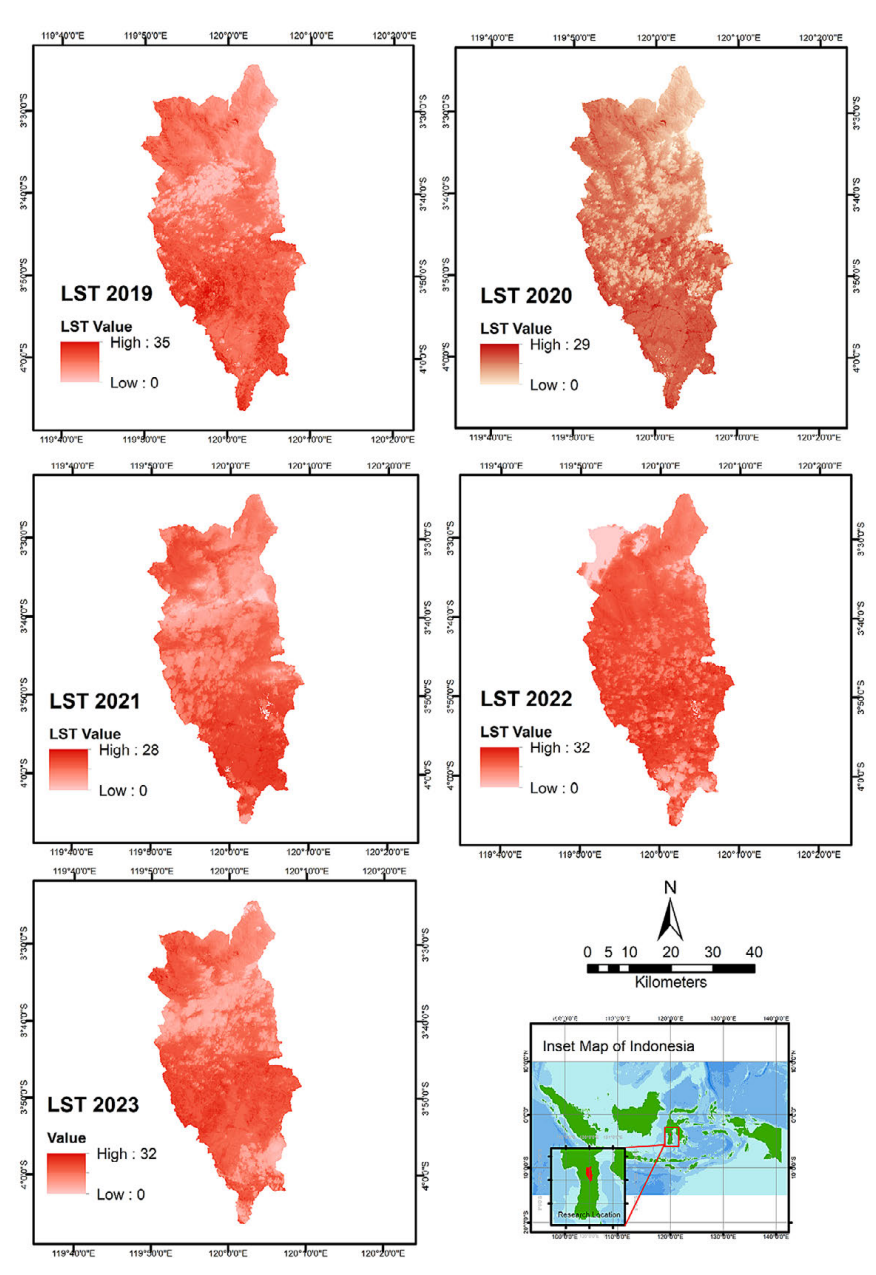


Figure 8. LST in the Bila Watershed, south Sulawesi, Indonesia, between 2019 and 2023 (Landsat 8)

Table 1. FR values of drought-causing factors

Factor	Factor Class	Pixel dryness (PxcL)	%PxcL	Pixel class factor (PnxL)	%PnxL	FR
Rainfall	1.500–2.000 mm year-1	340.862	92.57	834.635	47.31	1.96
Kaliliali	>3.000 mm year ⁻¹	27.346	7.43	929.631	52.69	0.14
Land cover	Water	3.005	0.82	26.617	1.51	0.54
	Open area	246	0.07	421	0.02	2.80
	Scrubs	11.675	3.17	222.912	12.63	0.25
	Primary forest	11	0.00	412.016	23.35	0.00
	Savannah/Grassland	5.300	1.44	11.959	0.68	2.12
	Paddy field	175.182	47.58	395.434	22.41	2.12
	Secondary forest	55	0.01	79.269	4.49	0.00
	Dryland agriculture	130.003	35.31	499.113	28.29	1.25
	Residential	35.330	9.60	58.516	3.32	2.89
	Mixed dryland area	6.699	1.82	56.349	3.19	0.57
	Swamp scrubs	442	0.12	1.172	0.07	1.81
	Plantations	260	0.07	488	0.03	2.55
	Nonbuilding (-1–0)	284.996	77.40	1.621.962	91.93	0.84
Building	Low (0-0.1)	40.635	11.04	70.893	4.02	2.75
density	Moderate (0.1–0.2)	35.524	9.65	57.142	3.24	2.98
	High (0.2–1)	7.053	1.92	14.269	0.81	2.37
	Very low (<-1)	186.803	50.73	793.231	44.96	1.13
	Low (-1-0)	131.393	35.68	721.658	40.90	0.87
Hotspot area	Moderate (0-1)	20.587	5.59	84.642	4.80	1.17
	High (1–2)	13.664	3.71	84.597	4.80	0.77
	Very high (>2)	15.761	4.28	80.138	4.54	0.94
	Non-vegetated (<0.125)	22.708	6.17	222.851	12.63	0.49
Vegetation	Sparse (0.125 – 0.25)	16.841	4.57	139.457	7.90	0.58
density	Moderate (0.25-0.5)	70.277	19.09	220.297	12.49	1.53
	Dense (>0.5)	258.382	70.17	1.181.661	66.98	1.05
Slope	Flat slope (0–8%)	229.859	62.43	556.588	31.55	1.98
	Sloping (8–15%)	84.570	22.97	250.926	14.22	1.61
	Moderately steep (15–25%)	34.969	9.50	201.337	11.41	0.83
	Steep slope (25–45%)	13.972	3.79	330.762	18.75	0.20
	Very steep slope (>45%)	4.838	1.31	424.653	24.07	0.05
River distance	<500 m	118.935	32.30	495.623	28.09	1.15
	500–2500 m	216.774	58.87	1.078.270	61.12	0.96
	>2500 m	32.499	8.83	190.373	10.79	0.82

period occurred in 2019, likely triggered by the El Niño phenomenon.

FR model

All values in Table 1 are not direct outputs from the spatial analysis process described in the method section. The number of drought event pixels in each pcator class (PxcL) was obtained through Extarct Multi-Value to Points, while the

total number of pixels in each factor class (PnxL) was calculated using raster statistics. These two values were the used in Equation 3 to calculate the FR value.

The results of the FR analysis showed that the occurrence of drought in the Bila watershed was mainly influenced by the density of buildings with moderate categories (FR = 2.98), land cover in the form of residential (FR = 2.89), and open area (FR = 2.80). This indicates that

built-up areas such as high-density residential are more sensitive to drought due to the impermeable nature of the surface (waterproof) causing low infiltration. In addition, the built-up area has a large heat absorption capacity, reflected in the high surface temperature value so as to accelerate the evaporation process. On the other hand, densely populated areas increase the pressure on household water needs, contributing to the water deficit, especially in the dry season. Meanwhile, open areas without vegetation on it also have a low water absorption capacity so that the availability of groundwater is limited. These findings are in line with the results of research by Alademomi et al. (2022) and Vinh et al. (2020), who reported that an increase in NDBI values, an indicator of the expansion of built areas, including housing, contributes to increasing soil surface temperatures, thereby increasing the risk of drought. In addition, open regions also contribute to worsening drought conditions. The lack of vegetation cover in these areas leads to relatively high evaporation rates. Research by Sarminah et al. (2019) reported that the evaporation rate in open regions reached 80% on the basis of the water balance approach using lysimeters.

Drought vulnerability

The values in Table 2 are derived from drought susceptibility index (DSI) raster generated from the sum all FR rasters. Classification was the performed using the Natural Breaks (Jenks) method in GIS software, and the number of pixels and area of each class were obtained automatically through raster statistics.

On the basis of the DSI results derived from the FR values, the drought vulnerability map (Figure 9) reveals that area with moderate to very high vulnerability is concentrated in the downstream region. In contrast, the upstream areas are mostly included in the low to very low vulnerability class.

High vulnerability in the downstream part of a watershed is associated mainly with types of land cover, such as rice farming and dryland farming. The findings of this study are supported by previous research. For example, Wicitra et al. (2023) examined the dynamics of soil surface temperature during the 2020-2023 drought in Kedungbanteng village, Tegal. They reported that high surface temperatures, an indication of drought, were concentrated in residential agricultural areas and drylands. Similarly, Hu et al. (2020) reported that the highest average surface temperature occurred in built-up areas (28.6 °C), followed by vacant land (26.0 °C) and dryland agriculture (25.8 °C). Although most of the downstream regions of the Bila watershed have high vegetation cover, this vegetation is dominated by crops, such as rice, which are highly dependent on rainfall and surface water availability, especially in rainfed farming systems. Thus, these areas remain vulnerable to drought.

In addition to agricultural areas, therapeutic areas also show high drought susceptibility. This is related to the increased water demand associated with higher building densities, especially in housing. Wada et al. (2013) emphasized that increased human water consumption significantly contributes to drought risk.

Data validation

The ROC validation performed by comparing DSI raster values at drought and non-srought points for both the training (70%) and validation (30%) datasets. The resulting ROC curves are shown in Figure 10, and the corresponding AUC values automatically generated from the SPSS ROC analysis are presented in Table 3.

Table 2. Drought vulnerability	class based	on DSI val	lues in the Bil	a watershed
---------------------------------------	-------------	------------	-----------------	-------------

DSI	Vulnerability categories	Number of pivole	Area	
DSI		Number of pixels	(ha)	(%)
3.11–4.88	Very low	620,463	56,436.44	35.54
4.88–6.92	Low	289,864	25,636.48	16.15
6.92–9.05	Moderate	313,681	28,183.99	17.75
9.05–11.01	High	432,380	38,944.97	24.53
11.01–13.62	Very high	107,878	9,582.16	6.03
Total		1,764,266	158,784.04	100.00

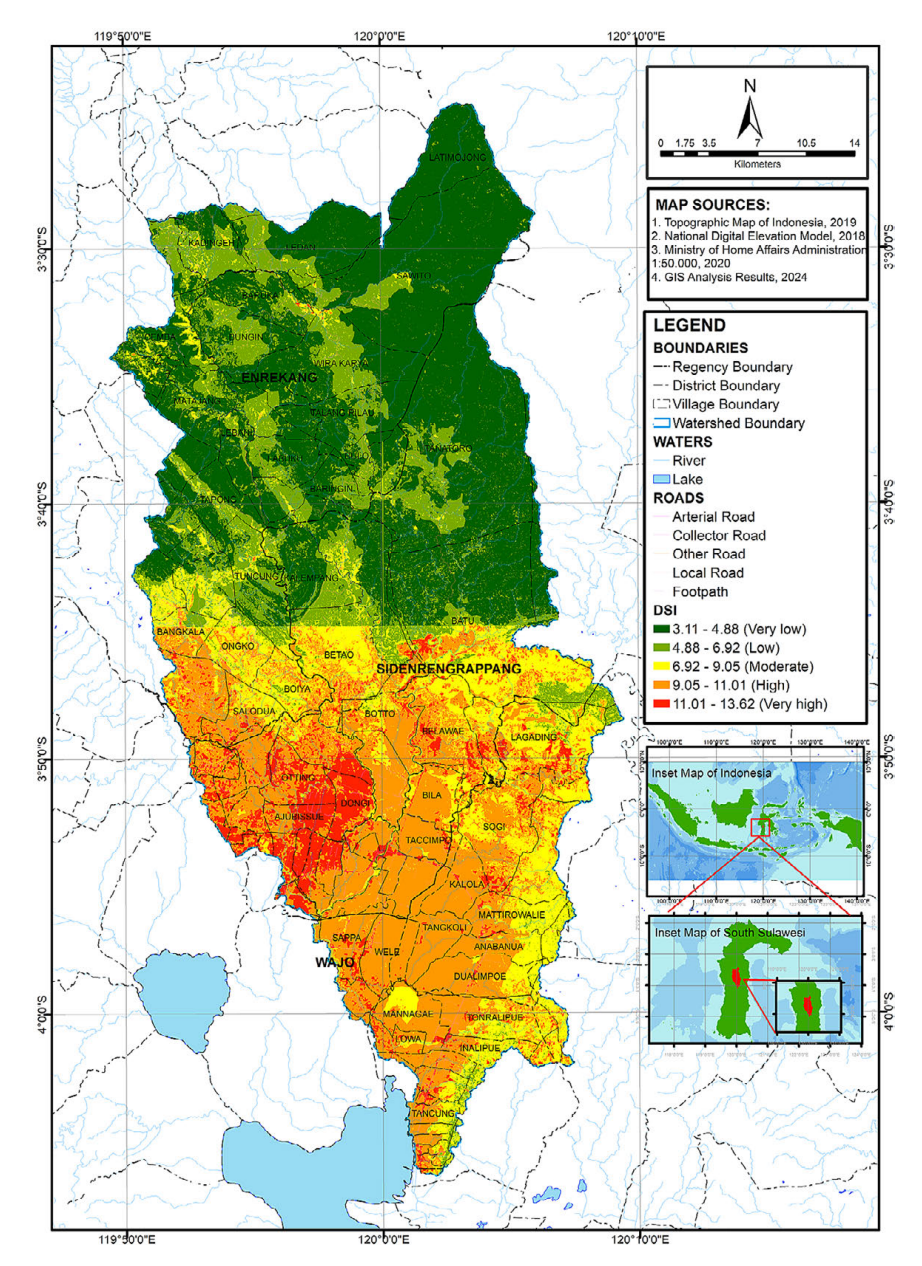


Figure 9. Drought vulnerability map based on DSI classification

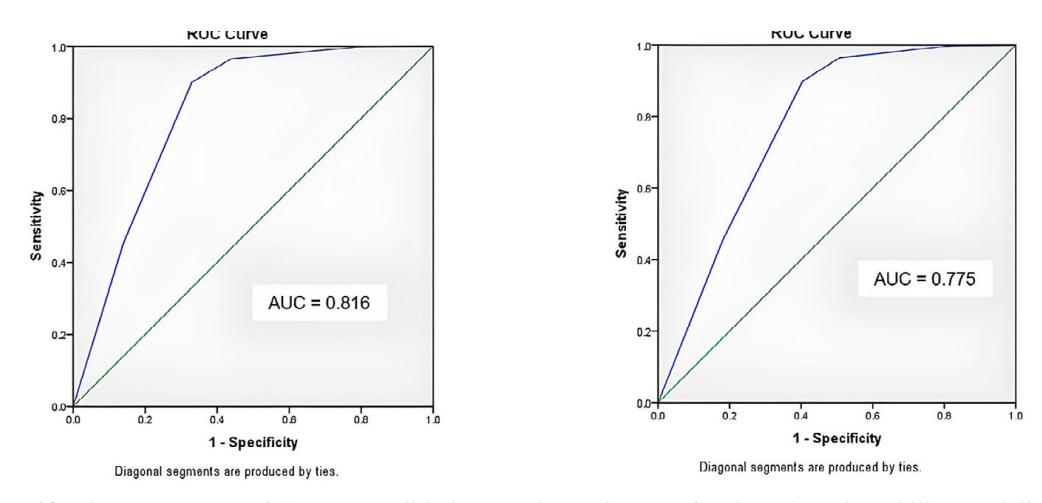


Figure 10. The AUC curve of the ROC validation results against FR for drought vulnerability modeling. (a) Success rate of the model. (b) Prediction rate of the model

Table 3. AUC values from the ROC validation results for the success rates and prediction rates of the FR models for drought susceptibility

AUC	AUC value	
Model success rate	0.817	
Model prediction rate	0.775	

Based on the AUC classification proposed by Balamurugan et al. (2017), the training dataset yielded an AUC value of 0.817, which shows excellent performance in recognizing the spatial patterns of historical drought events in the Bila watershed. This means that when evaluated with historical data, the model can identify drought-prone areas with increasing accuracy. Meanwhile, the validation dataset achieved an AUC value of 0.775, which indicates good predictive ability. This shows that when tested with independent (invisible) data, the model remains able to distinguish between drought and non-drought areas effectively.

The test of statistical significance of AUC values showed p < 0.05, which confirms that the model's predictive ability is significantly better than that of random classification (Ho: AUC = 0.5 is rejected). A small difference between the AUC values of training and validation (Δ AUC = 0.042) indicates that the model is stable and not overfitted, with good generalization capability for the Bila watershed region. Overall, these results suggest that the FR-based drought vulnerability model developed in this study provides reliable and reproducible predictions, and can serve as a valuable tool for spatial drought risk assessment and early warning planning in the region.

CONCLUSIONS

High surface temperatures have resulted in drought in the Bila watershed for more than five years. The affected areas are characterized by low rainfall, moderate building density, moderate vegetation density, and land cover types such as residential, paddy fields, plantations, and open areas, each of which has a high FR value. Drought-prone zone mapping revealed that areas with moderate to very high drought vulnerability are concentrated in the middle to downstream regions. In contrast, the low and very low drought vulnerability classes are concentrated on upstream areas. On the basis of the

vulnerability class in the Bila watershed, spatially differentiated adaptive mitigation strategies are recommended. The upstream-central zone focuses on vegetative measures such as reforestation, agroforestry, and afforestation to improve water infiltration and hydrological stability. In downstream zones, civil infrastructure, including infiltration wells, biopores, retention ponds, and drainage systems, should be prioritized and combined with mixed agroforestry to improve water uptake and reduce surface runoff. Densely populated areas encourage the development of green open spaces to lower local temperatures, increase rainwater infiltration, and increase local climate resilience.

Acknowledgments

The author would like to express his deepest gratitude to all the parties who supported this research.

REFERENCE

- Addis, A. (2023). GIS-based landslide susceptibility mapping using frequency ratio and shannon entropy models in Dejen District, Northwestern Ethiopia. *Journal of Engineering*, 2023. https://doi.org/ https://doi.org/10.1155/2023/1062388
- Ahmed, T., Singh, D. (2020). Probability density functions based classification of MODIS NDVI time series data and monitoring of vegetation growth cycle. *Advances in Space Research*, 66(4), 873–886. https://doi.org/10.1016/j.asr.2020.05.004
- 3. Alademomi, A. S., Okolie, C. J., Daramola, O. E., Akinnusi, S. A., Adediran, E., Olanrewaju, H. O., Alabi, A. O., Salami, T. J., Odumosu, J. (2022). The interrelationship between LST, NDVI, NDBI, and land cover change in a section of Lagos metropolis, Nigeria. *Applied Geomatics*, *14*(2), 299–314. https://doi.org/10.1007/s12518-022-00434-2
- Alonzo, C. A., Galabay, J. M., Macatangay, M. N., Magpayo, M. B., Ramirez, R. (2023). Drought risk assessment and monitoring of Ilocos Norte Province in the Philippines using satellite remote sensing and meteorological data. *AgriEngineering*, 5, 720–739. https://doi.org/https://doi.org/10.3390/ agriengineering5020045
- Amalo, L. F., Hidayat, R., Sulma, S. (2018). Analysis of agricultural drought in East Java using vegetation health index. *Agrivita*, 40(1), 63–73. https://doi.org/10.17503/agrivita.v40i1.1080

- 6. Avdan, U., Jovanovska, G. (2016). Algorithm for automated mapping of land surface temperature using LANDSAT 8 Satellite data. *Journal of Sensors*. https://doi.org/10.1155/2016/1480307
- Balamurugan, G., Seshan, K., Bera, S. (2017). Frequency ratio model for groundwater potential mapping and its sustainable management in cold desert, India. *Journal of King Saud University -Science*, 29(3), 333–347. https://doi.org/10.1016/j. jksus.2016.08.003
- 8. Cahyono, C., Juliastuti, Setyandito, O. (2024). Flood Analysis on Lake Tempe, South Sulawesi. *IOP Conference Series: Earth and Environmental Science*, *1343*(1), 1–8. https://doi.org/10.1088/1755-1315/1343/1/012019
- Cantarino, I., Carrion, M. A., Martínez-Ibáñez, V., Gielen, E. (2023). Improving landslide susceptibility assessment through frequency ratio and classification methods—case study of Valencia Region (Spain). *Apllied Science*, 13. https://doi.org/https:// doi.org/10.3390/app13085146
- Chuphal, D. S., Kushwaha, A. P., Aadhar, S., Mishra,
 V. (2024). Drought Atlas of India, 1901–2020. Scientific Data, 11(1), 1–12. https://doi.org/10.1038/s41597-023-02856-y
- 11. Cunha, A. P. M. A., Zeri, M., Leal, K. D., Costa, L., Cuartas, L. A., Marengo, J. A., Tomasella, J., Vieira, R. M., Barbosa, A. A., Cunningham, C., Cal Garcia, J. V., Broedel, E., Alvalá, R., Ribeiro-Neto, G. (2019). Extreme drought events over Brazil from 2011 to 2019. *Atmosphere*, 10(642). https://doi.org/10.3390/atmos10110642
- 12. Garg, V., Nikam, B. R., Thakur, P. K., Aggarwal, S. P., Gupta, P. K., Srivastav, S. K. (2019). Human-induced land use land cover change and its impact on hydrology. *HydroResearch*, *1*, 48–56. https://doi.org/10.1016/j.hydres.2019.06.001
- 13. Hasan, H. H., Razali, S. F. M., Muhammad, N. S., Ahmad, A. (2021). Hydrological drought across Peninsular Malaysia: Implication of drought index. *Natural Hazards and Earth System Sciences*, *June*, 1–28.
- 14. Hu, M., Wang, Y., Xia, B., Huang, G. (2020). Surface Temperature variations and their relationships with land cover in the Pearl River Delta. *Environmental Science and Pollution Research*, 27(30). https://doi.org/10.1007/s11356-020-09768-z
- 15. Islam, F., Ahmad, M. N., Janjuhah, H. T., Ullah, M., Islam, I. U., Kontakiotis, G., Skilodimou, H. D., Bathrellos, G. D. (2022). Modelling and mapping of soil erosion susceptibility of Murree, Sub-Himalayas using GIS and RS-based models Fakhrul. *Appllied Science*. https://doi.org/10.3390/app122312211
- 16. Lee, M., Kang, J., Jeon, S. (2012). Application of frequency ratio model and validation for predictive flooded area and susceptibility mapping using GIS.

- IGARSS, 1, 895–898.
- 17. Liviona, C. D. A., Saraswati, R., Wibowo, A. (2020). The Effect of NDVI and NDBI on Land Surface Temperature in Cirebon City 2015 and 2019. *E3S Web of Conferences*, 202. https://doi.org/10.1051/e3sconf/202020213006
- 18. Nursaputra, M., Pahar, S. P., and Chairil, A. (2021). Identification of drought level using normalized difference latent heat index in the south coast of South Sulawesi Province identification of drought level using normalized difference latent heat index in the South Coast of South Sulawesi Province. Earth and Environmental Science, 807. https://doi.org/10.1088/1755-1315/807/2/022032
- Prasetyo, D. A., Suprayogi, A., and Hani'ah. (2018).
 Analysis of Drought-prone Locations Using Geographic Information Systems in Blora Regency in 2017. *Journal of Undip Geodesy*, 7(4), 314–324.
- 20. Rahmat, S., Soma, A. S., Barkey, R. A. (2023). Land Cover Changes in Bila Watershed, South Sulawesi, Indonesia. *IOP Conference Series: Earth and Environmental Science*, 1230(1). https://doi.org/10.1088/1755-1315/1230/1/012045
- 21. Rahmati, O., Pourghasemi, H. R., Zeinivand, H. (2015). Flood susceptibility mapping using frequency ratio and weights-of-evidence models in the Golastan Province, Iran. *Geocarto International*, 37–41. https://doi.org/10.1080/10106049. 2015.1041559
- 22. Riajaya, P. D., Kadarwati, F. T., Hariyono, B., Subiyakto, Cholid, M. (2024). The Distribution of Rainfall in Areas Suitable for Sugarcane Farming in Blitar Regency, East Java. *IOP Conference Series: Earth and Environmental Science*, *1377*(1). https://doi.org/10.1088/1755-1315/1377/1/012012
- 23. Sarminah, S., Pasaribu, M., Aipassa, M. I. (2019). Estimation of evapotranspiration at agroforestri land and open area in educational forest of forestry faculty Unmul. *Agrifor*, 18(2), 325–338.
- 24. Senjani, M., Kusratmoko, E., Ristya, Y. (2020). Spatial Distribution of Drought Levels in Bantimurung District, Maros Regency, South Sulawesi Province. *E3S Web of Conferences*, *153*. https://doi.org/10.1051/e3sconf/202015302008
- 25. Shashikant, V., Shariff, A. R. M., Wayayok, A., Kamal, R., Lee, Y. P., Takeuchi, W. (2021). Utilizing TVDI and NDWI to Classify Severity of Agricultural Drought in Chuping, Malaysia. *Agronomy*, 11(6). https://doi.org/10.3390/agronomy11061243
- 26. Soma, A., Kubota, T. (2017). The performance of land use change causative factor on landslide susceptibility map in upper Ujung-Loe Watersheds South Sulawesi, Indonesia. *Geoplanning*, *4*(2), 157–170. https://doi.org/10.14710/geoplanning.4.2.157-170

- 27. Thomas, V., Albert, J. R. G., Hepburn, C. (2014). Contributors to the frequency of intense climate disasters in Asia-Pacific countries. *Climatic Change*, *126*(3–4), 381–398. https://doi.org/10.1007/s10584-014-1232-y
- 28. Utama, W., Indriani, R. F. (2021). Regional Physiographic Study for the Hydrology of Kali Lamong Watershed Area. *IOP Conference Series: Earth and Environmental Science*, *936*(1). https://doi.org/10.1088/1755-1315/936/1/012032
- 29. Vinh, N. Q., Khanh, N. T., Anh, P. T. (2020). The Inter-relationships Between LST, NDVI, NDBI in remote sensing to achieve drought resilience in Ninh Thuan, Vietnam. *Lecture Notes in Civil Engineering*, 80, 201–209. https://doi.

- org/10.1007/978-981-15-5144-4_15
- 30. Wada, Y., Van Beek, L. P. H., Wanders, N., Bierkens, M. F. P. (2013). Human water consumption intensifies hydrological drought worldwide. *Environmental Research Letters*, *8*(3). https://doi.org/10.1088/1748-9326/8/3/034036
- 31. Wang, Y., Fang, Z., Hong, H., Costache, R., Tang, X. (2021). Flood susceptibility mapping by integrating frequency ratio and index of entropy with multilayer perceptron and classification and regression tree. *Journal of Environmental Management*, 289. https://doi.org/https://doi.org/10.1016/j.jenvman.2021.112449
- 32. Wicitra, A. P., Hersugondo, H., Kepirianto, C.,